

# Towards single-atom detection on a chip

Peter Horak, Bruce G. Klappauf

*Optoelectronics Research Centre, University of Southampton, Southampton SO17 1BJ, UK*

Albrecht Haase, Ron Folman, Jörg Schmiedmayer

*Physikalisches Institut, Universität Heidelberg, D-69120 Heidelberg, Germany*

Peter Domokos

*Institut für Theoretische Physik, Universität Innsbruck, Technikerstr. 25, A-6020 Innsbruck, Austria*

E. A. Hinds

*Sussex Centre for Optical and Atomic Physics, University of Sussex, Brighton BN1 9QH, UK*

(Dated: October 30, 2018)

We investigate the optical detection of single atoms held in a microscopic atom trap close to a surface. Laser light is guided by optical fibers or optical micro-structures via the atom to a photo-detector. Our results suggest that with present-day technology, micro-cavities can be built around the atom with sufficiently high finesse to permit unambiguous detection of a single atom in the trap with 10  $\mu$ s of integration. We compare resonant and non-resonant detection schemes and we discuss the requirements for detecting an atom without causing it to undergo spontaneous emission.

PACS numbers: 42.50.Ct, 32.80.Pj, 03.75.Be

## I. INTRODUCTION

The subject of matter wave optics is advancing rapidly, driven both by the fundamental interest in quantum systems and by the prospect of new instruments based on the quantum manipulation of neutral atoms. The recent miniaturization of atom traps above microfabricated surfaces [1, 2] has opened the possibility of using neutral atoms to perform quantum information processing (QIP) on a chip. This technology is attractive because it appears robust and scalable, and because trapped neutral atoms can have long coherence times.

Experiments have shown that it is possible to trap, guide, and manipulate cold, neutral atoms in miniaturized magnetic traps above a substrate using either microscopic patterns of permanent magnetization in a film or microfabricated wire structures carrying current or charge. These atom chips can create potentials where atoms are confined strongly enough to consider implementing quantum logic gate schemes [3]. In the last year, several groups have been able to load atom chip micro-traps with Bose-Einstein condensates (BEC) [4], which may serve as a coherent source of qubits. A next important step for QIP is the detection of individual atoms on a chip with a signal-to-noise ratio better than unity in, say, 10  $\mu$ s. Here we propose that this can be achieved using very small optical cavities microfabricated on the chip, in which the presence of a single atom produces a sufficient response in the light field to permit detection.

Section II presents a generic mathematical model of atom detection in a cavity. In Secs. III and IV we discuss resonant and off-resonant detection. Section V deals with the forces acting on the atom due to the detection process. We give a numerical simulation of an atom crossing the detection cavity while moving in an atom guide.

In Sec. VI we discuss some practical aspects of making optical cavities and waveguides on an atom chip. We conclude in Sec. VII. Appendix A provides details of the particular model cavity used in our analysis.

## II. GENERIC MODEL

In this section we develop a model for a two-level atom coupled to the coherent light field in a microscopic cavity. The picture is essentially one already used to describe experiments in the strong coupling regime of cavity quantum electrodynamics (QED) [5, 6, 7], however, we are interested here in a different region of parameter space. Because the cavities of interest are small, with mirrors of limited reflectivity, the cavity decay rates  $\kappa$  are many orders of magnitudes faster than those of the best optical resonators. On the other hand, these short cavities can support stable modes that have extremely small waist size ( $\sim 1 \mu$ m), resulting in very strong atom-cavity coupling  $g$ . In such cavities even a small photon number can be sufficient to saturate the atomic transition, so we need to take nonlinear effects into account. The elements of the atomic density operator  $\rho$  satisfy the optical Bloch equations

$$\frac{d}{dt}\rho_{01} = (-\Gamma - i\Delta_a)\rho_{01} + g\alpha^*(\rho_{00} - \rho_{11}), \quad (1)$$

$$\frac{d}{dt}\rho_{11} = -2\Gamma\rho_{11} + g(\alpha^*\rho_{10} + \alpha\rho_{01}). \quad (2)$$

Here,  $2\Gamma$  is the decay rate of the excited atomic state,  $\Delta_a$  is the detuning of the driving laser from the atomic resonance, and  $g$  is the single-photon Rabi frequency at the position of the atom. For simplicity we will assume

in the following that the atom sits at an intensity maximum of the light. The light field in the cavity is treated classically, i.e., a coherent state is assumed at all times. The coherent state amplitude  $\alpha$  obeys the equation of motion

$$\frac{d}{dt}\alpha = (i\Delta_c - \kappa)\alpha + g\rho_{10} + \eta. \quad (3)$$

Here  $\Delta_c$  denotes the detuning of the driving laser from the cavity resonance. The decay rate of the cavity field is  $\kappa \equiv \kappa_T + \kappa_{loss}$ , made up of  $\kappa_T$  due to photons that pass through the cavity mirrors, and  $\kappa_{loss}$  due to photons that leave the cavity by other processes. The term  $\eta$  is the cavity pumping rate, related to the pumping laser power by  $\eta = \sqrt{j_{in}\kappa_T}$ , where  $j_{in}$  is the rate of photons incident on the cavity.

The stationary solutions for the light amplitude in the cavity and for the population of the atomic excited state are

$$\alpha = \frac{\eta}{(\kappa + \gamma) - i(\Delta_c - U)}, \quad (4)$$

$$\rho_{11} = \frac{g^2 N}{\Delta_a^2 + \Gamma^2 + 2g^2 N}, \quad (5)$$

where

$$\gamma = \frac{g^2 \Gamma}{\Delta_a^2 + \Gamma^2 + 2g^2 N}, \quad (6)$$

$$U = \frac{g^2 \Delta_a}{\Delta_a^2 + \Gamma^2 + 2g^2 N}, \quad (7)$$

and  $N = |\alpha|^2$  is the mean intracavity photon number. When the quantity  $2g^2 N$  is small (large) compared with  $\Gamma^2$ , we say that the atomic saturation is low (high). Note that Eq. (4) defines the stationary field amplitude only implicitly because  $\gamma$  and  $U$  depend on  $N$ . Hence this equation normally has to be solved numerically.

The presence of the atom is detected through its effect on the field amplitude  $\alpha$ . This is partly due to the spontaneous scattering, which adds  $\gamma$  to the cavity damping rate in Eq. (4), and partly to the coherent scattering, which adds  $-U$  to the cavity detuning. With the atom at resonance and unsaturated, the additional damping is  $g^2/\Gamma$  and the ratio of this to the intrinsic cavity damping is  $g^2/(\Gamma\kappa)$ , the cooperativity parameter of laser theory. This parameter is fundamental to the description of the atom-cavity interaction. When it is much smaller (larger) than unity, we describe the atom-cavity coupling as weak (strong). For a cavity of length  $L$ , it can be expressed as

$$\frac{g^2}{\Gamma\kappa} = 2\frac{\sigma_a}{A}n_{rt} \quad (8)$$

where  $\sigma_a = 3\lambda^2/(2\pi)$  is the resonant atomic interaction cross section for light of wavelength  $\lambda$ ,  $A$  is the cross section of the cavity mode at the position of the atom, and  $n_{rt} = c/(4L\kappa)$  is the average number of round trips of a cavity photon before its decay. (Provided the reflectivity

of the mirrors is close to 1, the finesse of the cavity is just  $4\pi n_{rt}$ ). This agrees with the naive expectation that the effect of the atom should depend on the fraction of the light within its cross section and should increase linearly with the number of times each photon passes the atom. Note however that Eq. (8) is restricted to beam waist sizes  $A$  that are more than a few times the cross section  $\sigma_a$  because it only holds within the dipole and paraxial approximations [8, 9]. Let us emphasize some important scaling properties of this quantity in the following.

(i) If the cavity decay rate is dominated by losses at a fixed number of material interfaces, then the number of round trips  $n_{rt}$  is independent of the cavity length. It follows from Eq. (8) that if the atom is at the center of the cavity and the waist area  $A$  is held constant, then  $g^2/(\Gamma\kappa)$  is also independent of the cavity length. In this case, if one scales the cavity length and detuning by  $L \rightarrow rL$  and  $\Delta_c \rightarrow \Delta_c/r$  but keeps the pump laser power and  $\Delta_a$  constant, then the detector signal-to-noise ratio (as discussed in the following sections) and the back-action on the atom during the measurement will remain unchanged.

(ii) Equation (8) suggests that, within the paraxial approximation, the beam cross section at the atomic position should be as small as possible to increase the coupling of the atom to the light. However, the beam divergence increases as the waist is made smaller, increasing the diffractive losses and other non-paraxial imperfections and reducing  $n_{rt}$ . Consequently the optimum value for  $A$  depends on the specific details of the cavity and its losses.

In the following two sections we will discuss two possible ways to detect the presence of an atom by measuring the output light beam. The first is to measure a dip in the output intensity using pump light that is resonant with the atom. The second is to measure the phase shift of the output light using an off-resonant pump. The more general case, in which an atom changes both the amplitude *and* the phase of the output beam, can be qualitatively understood by considering these two extremes.

### III. RESONANT ATOM DETECTION

Let us compare the number of resonant photons transmitted in a time  $\tau$  through the output mirror to a detector, with and without an atom in the cavity. For a given intra-cavity photon number  $N$  in a symmetric cavity, the number of photons arriving at the detector is  $N_{out} = N\kappa_T\tau$ . (This can be enhanced to  $2N\kappa_T\tau$  if the input mirror has much higher reflectivity than the output mirror). We are thus interested in the difference  $N_{out,0} - N_{out}$  where  $N_{out,0}$  is the output of the empty cavity. This signal must be compared to the quantum noise of the measurement, i.e. to the width  $\sqrt{N_{out}}$  of the Poissonian photon number distribution of a coherent state. The signal-to-noise ratio of this measurement scheme is

therefore

$$S = \frac{N_{out,0} - N_{out}}{\sqrt{N_{out}}}. \quad (9)$$

We will be interested in the regime  $N_{out,0} > 1$ . With the cavity and the atom both at resonance, the atomic transition saturates at very low intra-cavity photon number making the difference signal weak, so it is natural to consider using off-resonant excitation at higher intensity. However, it can be shown that  $S$  is maximum for resonant pumping and we will therefore pursue the idea of using  $\Delta_c = \Delta_a = 0$  in the following. Sensitive detection with detuning requires a more sophisticated homodyne technique, which we discuss in Sec. IV.

With  $\Delta_c = \Delta_a = 0$ , analytical solutions of Eq. (9) can be found for some limiting cases. In the limit of low atomic saturation, where  $2g^2N \ll \Gamma^2$ , we find

$$S = \sqrt{j_{in}\tau} \frac{g^2}{\kappa\Gamma} \frac{\kappa_T}{\kappa} \times \begin{cases} 2 & \text{for } \left(\frac{g^2}{\kappa\Gamma}\right) \ll 1 \\ 1 & \text{for } \left(\frac{g^2}{\kappa\Gamma}\right) \gg 1 \end{cases} \quad (10)$$

Hence the signal-to-noise ratio at low saturation increases with the square root of the incident laser power and integration time, but linearly with the number of photon round trips in the cavity. Losses also degrade the sensitivity through the factor  $\kappa_T/\kappa$ . In the opposite limit of strong saturation, where  $2g^2N \gg \Gamma^2$ , Eq. (4) yields

$$N = \frac{\eta^2}{\kappa^2} - \frac{\Gamma}{\kappa} \quad (11)$$

which gives

$$S = \Gamma \sqrt{\frac{\tau}{j_{in}}}. \quad (12)$$

Thus the signal-to-noise ratio *decreases* with the square root of the intensity when the transition is saturated. This is because the noise due to fluctuations of  $N_{out}$  approaches  $\sqrt{j_{in}\tau}$ , whereas the number of photons scattered by the atom is limited to  $\Gamma\tau$ . This result is independent of all the cavity parameters.

In Figures 1 and 2 we show some numerical results based on resonant pumping of the simple cavity described in Appendix A. Figure 1(a) shows the output photon number as a function of the pump power, both with and without an atom in the cavity. With an empty cavity, the output is proportional to the pump power for all parameters. With an atom in the cavity this scaling also holds as long as the atomic saturation is small. For the parameters chosen here the atom-light coupling is strong, i.e.,  $g^2 \gg \kappa\Gamma$ , and thus the atom significantly reduces the intra-cavity photon number as long as it is not saturated. For strong atomic saturation we find that  $N_{out,0}$  and  $N_{out}$  differ by a constant value, in accordance with the second term of Eq. (11). In Fig. 1(b) we plot the signal-to-noise ratio  $S$  versus pumping for three different values of  $\kappa_T$ . In each case,  $S$  increases with  $\sqrt{j_{in}}$  for

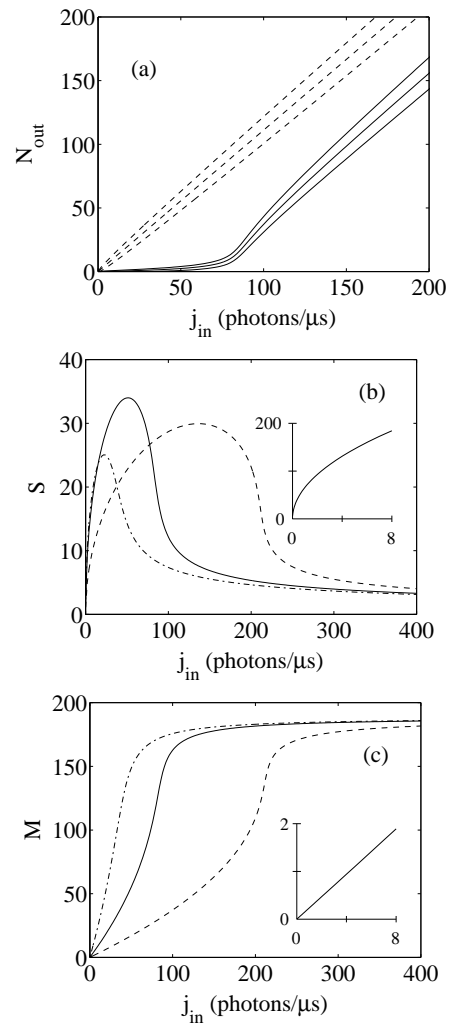


FIG. 1: Resonant detection of a single Rb atom with  $(g, \Gamma, \kappa_{loss}) = 2\pi \times (12, 3, 6)$  MHz,  $\tau = 10 \mu s$ . (a) Number  $N_{out}$  of photons transmitted through the cavity with (solid line) and without (dashed) atom. Thin lines correspond to shot noise,  $\kappa_T = 2\pi \times 3$  MHz. (b) Signal-to-noise ratio  $S$  for  $\kappa_T/(2\pi) = 1$  MHz (dashed), 3 MHz (solid), and 10 MHz (dash-dotted). Inset:  $S$  for a better cavity with  $\kappa_{loss} = \kappa_T = 2\pi \times 0.59$  MHz. (c) Number  $M$  of photons emitted spontaneously by the atom during the measurement [parameters as in (b)]. The parameters are justified by calculations performed in appendix A for an experimentally feasible cavity.

weak fields and then decreases in stronger fields in accordance with Eqs. (10) and (12). The optimum sensitivity, observed close to atomic saturation ( $2Ng^2 \approx \Gamma^2$ ), is obtained at a different pump power on each curve. There is also an optimum value for the mirror transmission. We found numerically that this occurs at  $\kappa_T \approx \kappa_{loss}/2$  with strong coupling and  $\kappa_T \approx \kappa_{loss}$  with weak coupling. For the parameters given, a single atom can be detected with signal-to-noise ratios of up to 35.

Figure 1(c) shows  $M \equiv 2\Gamma\tau\rho_{11}$ , the number of photons spontaneously scattered by the atom during the detection

process. With the parameters used here, smaller  $\kappa_T$  gives smaller  $M$  at a given pump power, but this depends on the value of  $\kappa_{loss}$  and is not always so. For example,  $M \propto 1/\kappa_T$  when  $\kappa_{loss} = 0$  and the coupling is weak. In the strongly saturated regime, all curves converge to the limit  $M = \Gamma\tau$ . This spontaneous scattering causes momentum diffusion of the atom and loss of atomic coherences. For the purpose of atom detection, this does not constitute a problem. However, if one had in mind to use the atom-cavity coupling for reversible, quantum logic operations it would be essential to have little or no spontaneous decay. One would then approach the regime of so-called interaction-free measurements [10, 11, 12]. Atomic motion will be discussed in more detail in Sec. V. In the weak saturation regime we can use Eq. (10) to express  $M$  as a function of the signal-to-noise ratio,

$$M = S^2 \frac{\kappa}{\kappa_T} \times \begin{cases} \frac{1}{2} \left( \frac{g^2}{\kappa\Gamma} \right)^{-1} & \text{for } \left( \frac{g^2}{\kappa\Gamma} \right) \ll 1 \\ 2 \left( \frac{g^2}{\kappa\Gamma} \right)^{-3} & \text{for } \left( \frac{g^2}{\kappa\Gamma} \right) \gg 1 \end{cases} \quad (13)$$

Hence with weak coupling and fixed signal-to-noise ratio, the number of spontaneously scattered photons is inversely proportional to the number of round trips  $n_{rt}$ . This is because the probability of the atom scattering a given photon is directly proportional to  $n_{rt}$ . In the strong coupling regime, on the other hand, the behavior is nonlinear and  $M \propto 1/n_{rt}^3$ . Therefore an increase of  $n_{rt}$  by a factor of 10 would reduce the photon scattering by three orders of magnitude. Of course, the increase of  $n_{rt}$  also reduces the number of photons in the cavity output. When  $\kappa_{loss}$  and  $\kappa_T$  are reduced to  $2\pi \times 0.59$  MHz and  $j_{in} = 2$  photons/ $\mu s$ , we find  $N_{out,0} = 5$  and  $M = 0.47, S = 93$ , as shown in the insets of Figs. 1(b) and (c).

Figure 2 is similar to Fig. 1 but with four larger values of  $\kappa_{loss}$  and with  $\kappa_T$  set equal to  $\kappa_{loss}/2$  in each case so as to achieve optimum signal-to-noise ratio. The curves for  $S$  and  $M$  as a function of the pump power are generally similar to Fig. 1, but in accordance with the lower cavity finesse, the maximum values of  $S$  are reduced. These curves correspond approximately to additional losses of 1%, 2%, 4%, and 10% per round trip of the cavity, as described in Appendix A. For the largest loss rate,  $\kappa_{loss} = 2\pi \times 86$  MHz and the maximum value of  $S$  is 3.75. At this point the number of scattered photons is  $M = 86$ , which amounts to a considerable disturbance of the atom. For lower loss rates, on the other hand, large signal-to-noise ratios can be achieved with only few photon scattering events.

The possibility of a large signal-to-noise ratio with few scattered photons makes this cavity-based detection method more attractive than standard resonance fluorescence imaging. Consider a simple resonance fluorescence setup where two light guides are mounted on the chip at 90 degrees to each other. One guides laser light to the atom trapped above the chip, while the second receives scattered photons and conveys them to a photodetector.

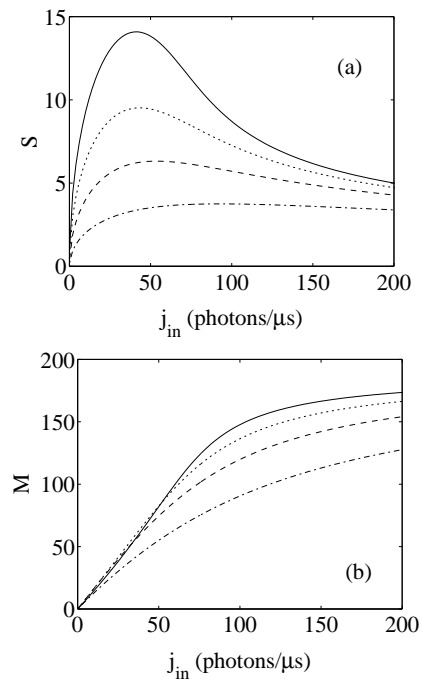


FIG. 2: Same as Fig. 1 but with increased loss rates  $\kappa_{loss}/(2\pi) = 14$  MHz (solid line), 22 MHz (dotted), 38 MHz (dashed), 86 MHz (dash-dotted). Again  $\tau = 10 \mu s$ . For each curve  $\kappa_T = \kappa_{loss}/2$  to get optimum signal-to-noise ratios.

The second guide collects only a small fraction of the scattered light since its end subtends a small solid angle at the atom. For example, a guide with a  $10 \mu m$  core mounted  $10 \mu m$  away from the atom collects  $\sim 5\%$  of the total scattered photons. Hence an atom scatters at least 20 photons for every signal photon and there is no possibility of measuring the atom without disturbing it strongly.

#### IV. OFF-RESONANT DETECTION: HOMODYNE MEASUREMENT

In the previous section the cavity and the atom were pumped resonantly. We found in that case that atom detection without spontaneous scattering involves a very small cavity output except when the coupling is very strong. One might therefore suspect that the detection scheme could be improved by working with far off-resonant light, using the dispersive interaction to produce an optical phase shift. In this section we investigate that idea. We continue to take  $\Delta_c = 0$ , but now assume a large atom-pump detuning  $\Delta_a \gg \Gamma$  so that the scattering rate  $\gamma$  is much less than the light shift  $U$  [Eqs. (6),(7)]. In this situation the dominant effect of the atom is to shift the resonance frequency of the cavity, thereby changing the phase of the cavity output but not its amplitude.

Equation (4) can then be written as

$$\alpha \approx \frac{\eta}{\kappa + iU} = \frac{\eta}{\kappa} \frac{1}{1 - i\phi} \approx \frac{\eta}{\kappa} e^{i\phi} \quad (14)$$

where the phase shift

$$\phi = -\frac{U}{\kappa} \quad (15)$$

is assumed to be  $\ll 1$ .

A balanced homodyne detection scheme can measure the phase of the cavity output. The cavity output field is mixed with a strong local oscillator laser field on a 50-50 beam-splitter and the difference of the light intensities in the two beam-splitter output ports is measured. The quantum noise of the signal is determined by the noise of the strong local oscillator, the signal-to-noise ratio being given by

$$S_{hom} = 2\sqrt{N_{out}} |\sin \phi| \approx 2\sqrt{N_{out}} \frac{|U|}{\kappa}. \quad (16)$$

Because of the condition  $|\phi| \ll 1$ ,  $N_{out} = N_{out,0} = j_{in}\tau(\kappa_T/\kappa)^2$ . In the limit of low atomic saturation, we find

$$S_{hom} = 2\sqrt{j_{in}\tau} \frac{\kappa_T}{\kappa} \frac{g^2}{\Delta_a \kappa}. \quad (17)$$

Hence according to Eq. (8), the signal-to-noise ratio increases linearly with  $n_{rt}$ . Note also that  $S_{hom}$  is  $\Gamma/\Delta_a$  times the  $S$  of Eq. (10) for resonant detection; with the same pump strength the off-resonant  $S_{hom}$  is much smaller than the resonant  $S$ . For strong atomic saturation on the other hand, we obtain

$$S_{hom} = \Delta_a \sqrt{\frac{\tau}{j_{in}}} \quad (18)$$

which is larger than the corresponding result for resonant detection, Eq. (12), by a factor of  $\Delta_a/\Gamma$ . Again, this is independent of  $\kappa$ ,  $\kappa_T$ ,  $A$ , and  $n_{rt}$ .

The number of photons scattered spontaneously by the atom during the interaction time can be expressed in terms of  $S_{hom}$  as

$$M = S_{hom}^2 \frac{\kappa}{\kappa_T} \frac{1}{2} \left( \frac{g^2}{\Gamma\kappa} \right)^{-1}. \quad (19)$$

Therefore, in order to achieve a certain signal-to-noise ratio,  $M$  is the same for the homodyne detection scheme as it is in the weak-coupling limit of resonant detection (see Eq. 13). Note that the condition  $|\phi| \ll 1$  prevents us from reaching the nonlinear regime of strong coupling here. The number of photons transmitted through the cavity during this atom detection is larger by a factor of  $\Delta_a^2/\Gamma^2$  than it is in the resonant detection scheme:

$$N_{out} = \frac{1}{4} S_{hom}^2 \left( \frac{\Gamma\kappa}{g^2} \right)^2 \frac{\Delta_a^2}{\Gamma^2}. \quad (20)$$

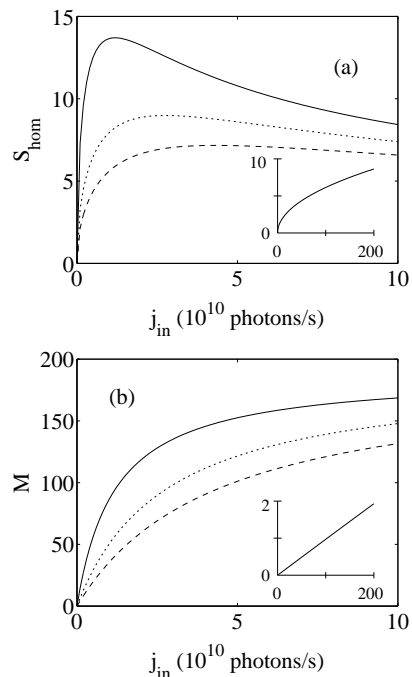


FIG. 3: Off-resonant atom detection using a homodyne measurement over  $\tau = 10 \mu\text{s}$ . (a) Signal-to-noise ratio  $S_{hom}$  and (b) number  $M$  of spontaneously scattered photons for  $\kappa_{loss}/(2\pi) = 6$  MHz (solid line), 14 MHz (dotted), and 22 MHz (dashed). For each curve  $\kappa_T = \kappa_{loss}$ .  $\Delta_a = 50\Gamma$ , other parameters as in Fig. 1. Insets:  $\kappa_{loss} = \kappa_T = 2\pi \times 0.59$  MHz,  $\Delta_a = 200\Gamma$ .

Figure 3(a) shows the homodyne detection signal-to-noise ratio  $S_{hom}$  as a function of the pump power. Comparing this with Fig. 1(b), we see that the maximum signal-to-noise ratio for the homodyne detection is smaller but of the same order of magnitude as for the resonant detection scheme. This agrees with the discussion above. The reduction by about a factor of two for the solid curve (lowest cavity loss rate) is due to the fact that we are limited to the weak coupling regime here and therefore do not benefit from the nonlinear effects of the strong coupling seen in Fig. 1(b). Moreover, we find numerically that  $S_{hom}$  is maximized for  $\kappa_T \approx \kappa_{loss}$ , i.e., for slightly larger mirror transmissions than for the resonant scheme. However, the pump intensity corresponding to maximum  $S_{hom}$  is much larger because of the large atom-pump detuning  $\Delta_a$ . Indeed, the main advantage of the homodyne detection scheme is that the signal consists of arbitrarily many photons compared to the few photons in the cavity output for some parameter regimes of Figs. 1 and 2. In Fig. 3(b) we depict the corresponding number  $M$  of spontaneously scattered photons. Again,  $M$  is found to be of the same order of magnitude as for the resonant detection scheme. This is because the reduced atom-photon coupling in the far-detuned limit is compensated by the larger number of photons used to achieve a good signal-to-noise ratio. The heating of

atomic motion and loss of atom coherence due to photon scattering are therefore similar in both the resonant and the off-resonant detection schemes. It follows from Eq. (19) that a large ratio of  $g^2/(\kappa\Gamma)$  is needed to make  $S_{hom} > 1$  and  $M < 1$ . With  $\kappa_{loss} = \kappa_T = 2\pi \times 0.59$  MHz and  $\Delta_a = 200\Gamma$ , for example, a pump current of 50 photons/ $\mu$ s gives  $N_{out,0} = 125$  and  $M = 0.49$ ,  $S_{hom} = 4.3$  as shown in the insets of Fig. 3.

## V. ATOMIC MOTION

Up to this point we have supposed that the atom is held by the magnetic microtrap at a maximum of the cavity field for the duration of the measurement time  $\tau$ . In this section we show that reliable detection is possible, even when the atom is allowed to move around within the light field. We consider a simple experiment in which the pump laser is continuously on, while single atoms traverse the cavity at random and have to be detected during their limited interaction time with the cavity field. Rubidium atoms trapped in an atom chip waveguide at a temperature of  $1\mu$ K move at typical thermal velocities of 1cm/s. Such an atom would typically take  $300\mu$ s to cross a  $3\mu$ m cavity mode waist if it were not interacting with the light. This is plenty of time to allow detection, being much longer than the  $\tau = 10\mu$ s interaction time assumed in previous sections of this paper. However, the interaction may impart some random momentum kicks to the atom. If this heating is too great, the atom may leave the interaction region before it can be detected, regardless of its initial velocity.

The broadening of the momentum distribution  $\Delta p$  over a time  $\tau$  is related to the momentum diffusion coefficient  $D$  through the relation  $(\Delta p)^2 = 2D\tau$ . For an atom in a standing wave cavity in the limit of weak atomic saturation ( $2g^2N \ll \Gamma^2$ ) we can use the value of  $D$  given in Refs. [13]. For simplicity we restrict the following discussions to the resonant case  $\Delta_a = \Delta_c = 0$ . Thus

$$D = \Gamma(\hbar k)^2 \frac{\eta^2 g^2}{[\Gamma\kappa + g^2 \cos^2(kz)]^2}, \quad (21)$$

where  $k$  is the wave vector of the light field,  $g$  is again the maximum Rabi frequency, and  $z = 0$  is at an antinode of the field. When  $z = 0$ ,  $2D\tau$  is equal to  $2\Gamma(\hbar k)^2 \rho_{11}\tau$ , which is just  $(\hbar k)^2 M$ . Hence, the momentum distribution of an atom at an antinode broadens by  $\Delta p = \hbar k \sqrt{M}$  during the interaction time. At this position, the condition  $M < 1$  for reversible atom-light interaction is also the condition for leaving the motional state of the atom unchanged. Away from the antinodes, however, this is no longer true. For example,  $M = 0$  at a node, while  $D$  is maximum. In this case, it is *coherent* scattering of photons between the forward and backward directions in the cavity that gives rise to the momentum diffusion [14]. However, in general the use of a cavity in atom detection reduces the heating of the atom significantly

compared with simple resonance fluorescence detection. Moreover, the counter-propagating fields in a cavity produce a much smaller mean scattering force than a single travelling beam, whose radiation pressure force can expel the atom quickly from the interaction region. In the ultimate limit of very large atom-cavity coupling (“interaction-free” measurement), the atomic motional state is completely unperturbed by the detection.

Let us now take this position dependence into account by simply averaging the results of Sec. III over the position along the cavity axis assuming a flat spatial distribution of the atom. For the spatially averaged signal-to-noise ratio  $\bar{S}$  at resonance we find

$$\begin{aligned} \bar{S} &= \sqrt{j_{in}\tau \frac{\kappa_T}{\kappa}} \left[ 1 + \frac{g^2}{2\kappa\Gamma} - \left( 1 + \frac{g^2}{\kappa\Gamma} \right)^{-1/2} \right] \\ &= \sqrt{j_{in}\tau \frac{g^2}{\kappa\Gamma} \frac{\kappa_T}{\kappa}} \times \begin{cases} 1 & \text{for } \left( \frac{g^2}{\kappa\Gamma} \right) \ll 1 \\ \frac{1}{2} & \text{for } \left( \frac{g^2}{\kappa\Gamma} \right) \gg 1 \end{cases} \quad (22) \end{aligned}$$

This is exactly half of the maximum value of  $S$  given by Eq. (10). The corresponding mean number  $\bar{M}$  of spontaneously scattered photons is

$$\begin{aligned} \bar{M} &= j_{in}\tau \frac{\kappa_T}{\kappa} \left( \frac{\kappa\Gamma}{g^2} \right)^{1/2} \left( 1 + \frac{\kappa\Gamma}{g^2} \right)^{-3/2} \\ &= j_{in}\tau \frac{\kappa_T}{\kappa} \times \begin{cases} \frac{g^2}{\kappa\Gamma} & \text{for } \left( \frac{g^2}{\kappa\Gamma} \right) \ll 1 \\ \left( \frac{g^2}{\kappa\Gamma} \right)^{-1/2} & \text{for } \left( \frac{g^2}{\kappa\Gamma} \right) \gg 1 \end{cases} \quad (23) \end{aligned}$$

We note that in the weak coupling limit, the dependence of  $\bar{M}$  on  $\bar{S}$  differs from Eq. (13) only by a factor of two, whereas it is qualitatively different in the strong coupling limit. The spatially averaged value  $\bar{D}$  of the momentum diffusion reads

$$\bar{D} = \frac{(\hbar k)^2}{\tau} \left( 1 + \frac{g^2}{2\kappa\Gamma} \right) \bar{M} \quad (24)$$

and thus the rms momentum change during detection is

$$\Delta p = \hbar k \sqrt{2\bar{M} \left( 1 + \frac{g^2}{2\kappa\Gamma} \right)}. \quad (25)$$

The corresponding random walk in position leads to a spatial spreading  $\Delta z$  of

$$\Delta z = \sqrt{\frac{2\bar{D}}{m^2} \frac{\tau^3}{3}} = \frac{\Delta p}{m} \frac{\tau}{\sqrt{3}}, \quad (26)$$

where  $m$  is the atomic mass. As an example, let us take the parameters of the dotted curve in Fig. 2 with  $j_{in} = 20$  photons/ $\mu$ s. Then  $\bar{S} = 5.1$ ,  $\bar{M} = 25$ ,  $\Delta p = 9.3\hbar k$ , and  $\Delta z = 320$  nm. Thus the heating and diffusive motion are relatively small and do not compromise the feasibility of single-atom detection.

We have performed numerical simulations of a simple experiment in which atoms move along a guide perpendicular to the cavity axis and cross the cavity field. The

parameters used are  $(g, \Gamma, \kappa_{loss} = \kappa_T) = 2\pi \times (12, 3, 14)$  MHz,  $j_{in} = 10$  photons/ $\mu s$ , and cavity waist  $w_0 = 3 \mu m$ . The transverse oscillation frequency in the guide is  $2\pi \times 37$  kHz, the atoms move along the guide with a mean velocity of 0.4 m/s, and the initial temperature of the cloud before interaction with the cavity is  $30 \mu K$ . Here the motion of the atoms is classical. It is beyond the scope of the present paper to consider single atoms magnetically trapped in the Lamb-Dicke regime or to analyze the effect of the cavity field on a Bose-Einstein condensate.

Figure 4(a) shows the typical temporal evolution of the intra-cavity photon number  $N$  in one particular realization of the simulation. It is constant as long as there is no atom interacting with the cavity mode, but with the arrival of an atom,  $N$  exhibits periods of strong reduction according to the position of the atom within the cavity. This curve has been used to simulate the arrival times of individual photons at the photo-detector measuring the cavity output. Detector clicks are indicated by the vertical lines at the bottom of Fig. 4(b) and the scarcity of clicks near time  $t \approx 45 \mu s$  indicates the presence of the atom. This appears even more clearly in the solid line of Fig. 4(b), which plots the number of photons arriving in an  $8 \mu s$  integration window versus time. For comparison, the dashed lines show the corresponding mean number of photons, plus and minus one standard deviation, when there is no atom in the cavity. A simple criterion for the detection of an atom in the cavity would thus be to define a minimum value for  $N_{detect}$  and infer the presence of an atom whenever the curve drops below that. With the minimum set at 11, we found that this procedure detects 77% of the atoms, while the shot noise of the cavity field produces only 750 false atoms per second. Note that a higher threshold increases the detection efficiency, but simultaneously increases the dark count rate. In practice, a more sophisticated data analysis could provide better discrimination between real detection events and dark counts. On average, each atom makes  $M = 28.3$  spontaneous emissions, a result quite comparable to the simple 1D averages discussed above.

## VI. MICRO CAVITY DESIGN

It is beyond the scope of this paper to consider the details of specific micro-cavity designs, but it does seem appropriate to make some general remarks about the feasibility of building suitable cavities. In this work, we are not thinking of whispering gallery cavities [15], where the light is trapped near the perimeter of a small sphere or disk and atoms may couple to the evanescent field that leaks out. Rather, we have in mind an open resonator in which atoms can have access to the regions of maximum optical field. The lower Q of the open resonator can be compensated by the small waist size of the cavity mode, which we are taking to be a few  $\mu m$ .

A simple cavity of this kind might be made using a

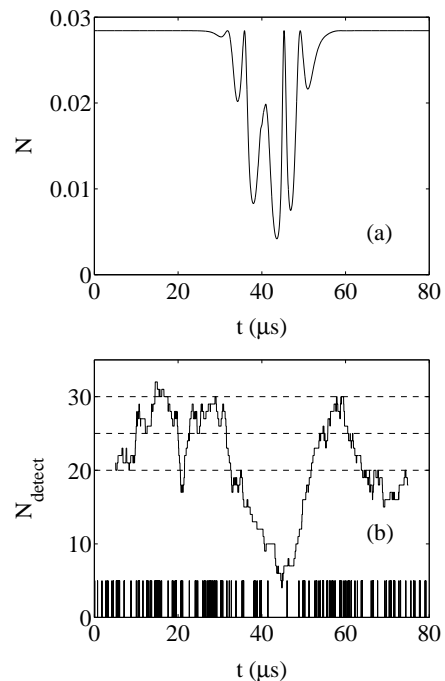


FIG. 4: Numerical simulation of an atom which is trapped in a 2D harmonic trap but moves along the third dimension and traverses the cavity. (a) Stationary intra-cavity photon number  $N$  vs. time. (b) Simulated detector signal vs. time: arrival time of individual photons at the photo-detector (vertical lines at bottom), number of detected photons integrated over intervals of  $8 \mu s$  (solid line), mean integrated photon number for an empty cavity and corresponding quantum noise (dashed). (See text for details.)

pair of optical fibers, each with an integrated Bragg reflector. The two fibers, aimed at each other with a small gap between the ends, form a cavity, see Fig. 5. Of course there are reflections at the fiber ends and losses from the region of the gap as well as absorption in the fiber itself, but such a cavity has the virtue that it is easy to build and its modes are readily analyzed, which we do in appendix A. The damping and coupling parameters used in this work are realistic parameters for such a cavity, as calculated in the appendix. The gap where the atom is placed should be wide enough to avoid long-range van der Waals or Casimir-Polder interactions between the atom and the end of the fiber. These forces become problematic at distances below a few hundred nm [16, 17].

The cavity could be significantly improved by matching the ends of the fibers to the wavefronts in the gap. With this in mind we have demonstrated a fiber terminated by a microlens that produces a  $2 \mu m$  beam waist  $50 \mu m$  from the end of the fiber, but an analysis of the microlens cavity is beyond the scope of appendix A. GRIN rod lenses also lend themselves to this application. It is also desirable for the cavity to be tunable so that its mode frequencies can be properly chosen relative to the atomic transition of interest. Temperature tuning and piezoelectric tuning are both realistic options. Alternatively, the

cavity could be tuned electro-optically using, for example, a material such as lithium niobate ( $\text{LiNbO}_3$ ), whose refractive index changes by up to 1% in an applied electric field. Ultimately it is of interest to integrate optical structures for atom detection directly into the atom chip. Many dielectric and semiconductor materials combine suitable optical properties with low enough vapor pressure. Waveguides made from  $\text{SiN}$  or  $\text{Ta}_2\text{O}_5$  could be used in the red and near infrared for atoms such as Li and Rb, while GaAs structures would be appropriate for Cs.

## VII. CONCLUSIONS

In this work we have analyzed the use of optical microcavities for detecting single atoms on an atom chip. We find that even cavities of quite modest  $\kappa$ , in the range of  $2\pi \times 10$  MHz, can play a useful role provided the waist of the light field is only a few  $\mu\text{m}$ . With lower loss, such cavities permit the detection of a single atom while requiring less than 1 photon to be spontaneously scattered. The effect of optical dipole forces can be significant.

Our calculations show that the effect on the atom is approximately the same for resonant and far-detuned pump light if one wants to obtain a fixed signal-to-noise ratio for the same cavity parameters. On resonance, simple monitoring of the cavity output power can be used to detect the atom, but very small photon numbers must be used to achieve maximum signal-to-noise ratio. By contrast, off-resonant detection permits much larger pump power and therefore much larger cavity output, but in this case a more refined homodyne technique must be used to detect the presence of the atom in the cavity. These methods seem promising for the detection of single atoms on an atom chip.

### Acknowledgments

This work was supported by the European Union (Contract No. IST-1999-11055, ACQUIRE), the Deutsche Forschungsgemeinschaft (Schwerpunktprogramme ‘‘Quanteninformationsverarbeitung’’, ‘‘Wechselwirkungen in ultrakalten Atom- und Moleklgasen’’), the Landesstiftung Baden-Wuerttemberg (Kompetenznetzwerk ‘‘Quanteninformationsverarbeitung’’), and the British Engineering and Physical Sciences Research Council. P. D. was supported by the European Commission (Contract No. HPMF-CT-2000-00788).

### APPENDIX A: MODES OF A FIBER GAP CAVITY

In this appendix we calculate the modes and loss rates of the simple fiber cavity used to illustrate the main part of the paper. The cavity consists of two single-mode

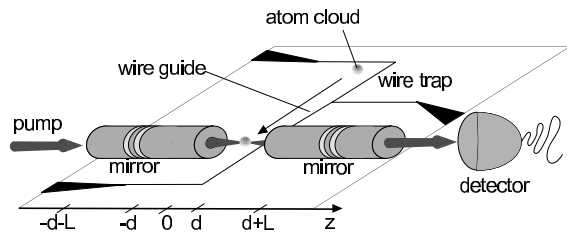


FIG. 5: Schematic presentation of the fiber cavity on an atom chip.

fibers mounted on top of the chip and placed on opposite sides of the current carrying wire that forms the magnetic atom trap. The guided atoms pass through a gap of length  $2d$  between the fibers, as illustrated in Fig. 5. Each fiber contains a highly reflective mirror, e.g. a Bragg reflector, at a distance  $L$  from its end. The cavity mode confined between these mirrors is concentrated in the fiber cores and in the gap between the fibers. As we show below, it is advantageous to use relatively large core diameters to reduce the energy loss by the mode mismatch between the fibers. The assumption of a single mode fiber thus leads to the requirement of a very small difference of the index of refraction between the fiber core and cladding. In this limit, the mode in the fiber can be well approximated by a transversely polarized field with a Gaussian profile of waist  $w_0$  [18]. Similarly, the paraxial approximation can be applied to the light field in the gap which is therefore Gaussian.

Thus, the electric field of the cavity mode can be written as

$$\mathbf{E}(\mathbf{x}) = \mathbf{e}_0 \times \begin{cases} A_{1+}f_{1+}(\mathbf{x}) + A_{1-}f_{1-}(\mathbf{x}) & \text{for } z < -d, \\ A_{2+}f_{2+}(\mathbf{x}) + A_{2-}f_{2-}(\mathbf{x}) & \text{for } |z| < d, \\ A_{3+}f_{3+}(\mathbf{x}) + A_{3-}f_{3-}(\mathbf{x}) & \text{for } z > d \end{cases} \quad (\text{A1})$$

where  $\mathbf{e}_0$  is the polarization vector,  $\mathbf{x}$  symbolizes the cylindrical coordinates  $(r, \varphi, z)$ , and

$$f_{1\pm}(\mathbf{x}) = e^{-r^2/w_0^2} e^{\pm ik_1(z+d)}, \quad (\text{A2})$$

$$f_{3\pm}(\mathbf{x}) = e^{-r^2/w_0^2} e^{\pm ik_1(z-d)}, \quad (\text{A3})$$

are the fiber modes traveling to the right (+) and left (-) within each of the two fibers. In the gap where the atoms are guided, the Gaussian beams emerging from the left (right) fiber and propagating to the right (left) are given by

$$f_{2+}(\mathbf{x}) = \frac{w_0}{w(z+d)} \exp \left[ -\frac{r^2}{w^2(z+d)} + ik_0 \frac{r^2}{2R(z+d)} + ik_0(z+d) - i\eta(z+d) \right], \quad (\text{A4})$$

$$f_{2-}(\mathbf{x}) = \frac{w_0}{w(z-d)} \exp \left[ -\frac{r^2}{w^2(z-d)} - ik_0 \frac{r^2}{2R(z-d)} - ik_0(z-d) + i\eta(z-d) \right]. \quad (\text{A5})$$



Here

$$\begin{aligned} w(z) &= w_0 \sqrt{1 + (z/z_0)^2}, \\ R(z) &= z[1 + (z_0/z)^2], \\ \eta(z) &= \arctan(z/z_0), \\ z_0 &= \pi w_0^2 / \lambda_0. \end{aligned} \quad (\text{A6})$$

Because of the divergence of the Gaussian beams in the gap,  $f_{2+}$  ( $f_{2-}$ ) does not exactly match the fiber mode  $f_{3+}$  ( $f_{1-}$ ) at  $z = d$  ( $z = -d$ ). Therefore we project  $f_{2\pm}$  onto  $f_{2\mp}^*$  at these positions and treat the mode mismatch as cavity loss. We find

$$\begin{aligned} f_{2-}(r, z = -d) &= Q f_{2+}^*(r, z = -d) + f_{2-}^\perp(r, z = -d), \\ f_{2+}(r, z = d) &= Q f_{2-}^*(r, z = d) + f_{2+}^\perp(r, z = d), \end{aligned}$$

where the coefficient  $Q$  gives the mode-matched part of the amplitude, while the superscript  $\perp$  indicates the part of the field that is orthogonal to the mode of the fiber and is therefore lost. We find that

$$Q = |Q| e^{i\phi} = \frac{w_0}{w(d)} e^{ik_0 2d - i\eta(d)}. \quad (\text{A7})$$

The phase of  $Q$  is of first order in  $d/z_0$ , i.e., gap size divided by twice the Rayleigh length, whereas the modulus of  $Q$  is of second order. We will therefore calculate the cavity modes in perturbation theory in  $d/z_0$ . The first order terms yield a change of the optical path length and hence a change of the resonance frequencies, but still allow for self-consistent, lossless modes, which can then be used in the second order terms to calculate the leading contribution of the cavity loss rate.

Using the continuity equations for the electric field at the fiber-vacuum interface together with the boundary conditions at the mirrors, we obtain the cavity resonance condition

$$d \left( 2k_0 - \frac{1}{z_0} \right) = m\pi - 2 \arctan \left[ \frac{1}{n} \tan(k_1 L) \right], \quad (\text{A8})$$

where  $m$  is an integer number and  $n = k_1/k_0$  is the effective refractive index of the fiber. We also obtain relations between the electric field amplitudes  $A_{j,\pm}$ , in particular

$$\begin{aligned} |A_{1+}| &= |A_{1-}| = |A_{3+}| = |A_{3-}| \quad (\text{A9}) \\ |A_{2+}| &= |A_{2-}| \\ &= |A_{1+}| \left| \frac{1 + n - (1 - n)e^{-2ik_1 L}}{2} \right|. \quad (\text{A10}) \end{aligned}$$

The energy flow in  $z$  direction in the gap is given by

$$S_z = \frac{\pi w_0^2 |A_{2+}|^2}{\mu_0 c} \quad (\text{A11})$$

which leads to a loss of energy from the cavity

$$S_{loss} = 2S_z(1 - |Q|^2). \quad (\text{A12})$$

If we divide this by the total energy of the light stored in the fiber cavity,  $E = 4n^2 \epsilon_0 \pi L w_0^2 |A_{1+}|^2$  (neglecting the small energy stored in the gap), we obtain the energy loss rate

$$2\kappa_{gap} = \frac{c}{2L} \left( \frac{d}{z_0} \right)^2 \left| \frac{1 + n - (1 - n)e^{-2ik_1 L}}{2n} \right|^2 \quad (\text{A13})$$

due to the mode mismatch of the mode coupling through the gap. The loss rate  $\kappa_{loss}$  is then the sum of  $\kappa_{gap}$  and any additional loss rates, e.g., due to material absorption. Finally, the maximum single photon Rabi frequency, observed for an atom on the axis of the cavity in the gap, is given by

$$g = |1 + n - (1 - n)e^{-2ik_1 L}| \sqrt{\frac{3\Gamma c}{2n^2 L w_0^2 k_0^2}}. \quad (\text{A14})$$

As an example let us consider rubidium atoms ( $\lambda_0 = 780$  nm) in such a cavity with  $L = 20000\lambda_1$ , which yields a node of the electric field at the fiber ends and therefore a large field in the gap, see Eq. (A10). The gap size is chosen as  $2d = 5.079 \mu\text{m}$  in accordance with the resonance condition (A8). The fiber core diameter is  $5 \mu\text{m}$ , the refractive index of the fiber core is  $n_1 = 1.5$ , and that of the cladding is  $n_2 = 1.496$ . For these parameters, the corresponding waist is  $w_0 = 2.92 \mu\text{m}$ ,  $\kappa_{gap} = 2\pi \times 6.23$  MHz and  $g = 2\pi \times 12.2$  MHz. A mirror transmission of  $T = 0.01$  gives  $\kappa_T = Tc/(4nL) = 2\pi \times 7.65$  MHz. This example motivates the choice of parameters used for the figures in this work. A smaller gap of  $2d = 1.563 \mu\text{m}$  gives  $\kappa_{gap} = 2\pi \times 0.59$  MHz, which we use in the insets of Figs. 1 and 3. Note that, as  $L$  is tunable, any experimental realization error concerning the exact magnitude of  $2d$  may be compensated in order to once again comply with the resonance condition (A8).

- 
- [1] E. A. Hinds and I. G. Hughes, J. Phys. D **32**, R119 (1999).  
 [2] R. Folman, P. Krueger, J. Schmiedmayer, J. Denschlag, and C. Henkel, Adv. At. Mol. Opt. Phys. **48**, 263 (2002).  
 [3] T. Calarco, E. A. Hinds, D. Jaksch, J. Schmiedmayer, J. I. Cirac, and P. Zoller, Phys. Rev. A **61**, 022304 (2000).

- [4] H. Ott, J. Fortagh, G. Schlotterbeck, A. Grossmann, and C. Zimmermann, Phys. Rev. Lett. **87**, 230401 (2001); W. Hänsel, P. Hommelhoff, T. W. Hänsch, and J. Reichel, Nature **413**, 498 (2001); A. E. Leanhardt, A. P. Chikkatur, D. Kielpinski, Y. Shin, T. L. Gustavson, W. Ketterle, and D. E. Pritchard, Phys. Rev. Lett. **89**,

- 040401 (2002); M. Jones *et al.*, submitted to Phys. Rev. A; S. Schneider *et al.*, submitted to Phys. Rev. A.
- [5] *Cavity Quantum Electrodynamics*, edited by P. R. Berman (Academic Press, Boston, 1994).
- [6] H. Mabuchi, Q.A. Turchette, M.S. Chapman, and H.J. Kimble, Opt. Lett. **21**, 1393 (1996).
- [7] P. Münstermann, T. Fischer, P. W. H. Pinkse, and G. Rempe, Opt. Commun. **159**, 63 (1999).
- [8] S. J. van Enk and H. J. Kimble, Phys. Rev. A **61**, 051802 (2000); *ibid.* **63**, 023809 (2001).
- [9] P. Domokos, P. Horak, and H. Ritsch, Phys. Rev. A **65**, 033832 (2002).
- [10] A. Elitzur and L. Vaidman, Found. Phys. **23**, 987 (1993).
- [11] P. Kwiat, H. Weinfurter, T. Herzog, A. Zeilinger, and M. A. Kasevich, Phys. Rev. Lett. **74**, 4763 (1995).
- [12] A. Karlsson, G. Björk, and E. Forsberg, Phys. Rev. Lett. **80**, 1198 (1998).
- [13] P. Horak, G. Hechenblaikner, K. M. Gheri, H. Stecher, and H. Ritsch, Phys. Rev. Lett. **79**, 4974 (1997); G. Hechenblaikner, M. Gangl, P. Horak, and H. Ritsch, Phys. Rev. A **58**, 3030 (1998).
- [14] J. P. Gordon and A. Ashkin, Phys. Rev. A **21**, 1606 (1980).
- [15] V. Lefevre-Seguin, Opt. Materials **11**, 153 (1999); D. W. Vernooy, A. Furusawa, N. Ph. Georgiades, V. S. Ilchenko, and H. J. Kimble, Phys. Rev. A **57**, R2293 (1998).
- [16] E. A. Hinds, Chapter 1 of Ref. [5].
- [17] J. Vuckovic, M. Loncar, H. Mabuchi and A. Scherer, Phys. Rev. E **65**, 016608 (2002).
- [18] G. P. Agrawal, *Fiber-optic communication systems* (John Wiley & Sons, New York, 1992).